Review copy – not for distribution

(pss-logo will be inserted here by the publisher)

1
2
3
4
5
6
7
8
9
10
11
12
13
14
15
16
17
18
19
20
21
22
23
24
25
26
27
28
29
30
31
32
33
34
35
36
37
38
39
40
41

Contactless electrical defect characterization in semiconductors by microwave detected photo induced current transient spectroscopy (MD-PICTS) and microwave detected photoconductivity (MDP)

Bastian Berger[1], Nadine Schüler[2], Sabrina Anger[2], Bianca Gründig-Wendrock[3], Jürgen R. Niklas[2], Kay Dornich[*,2]

[1] Institute of Theoretical Physics, TU Bergakademie Freiberg, Leipziger Straße, 09596 Freiberg, Germany
[2] Freiberg Instruments GmbH, Am St. Niclas Schacht 13, 09599 Freiberg, Germany
[3] SolarWorld Innovations GmbH, Berthelsdorfer Straße 111a, 09599 Freiberg, Germany

Received ZZZ, revised ZZZ, accepted ZZZ
Published online ZZZ (Dates will be provided by the publisher.)

Keywords electrical characterization, MDP, defects, lifetime

* Corresponding author: e-mail dornich@freiberginstruments.com, Phone: +49 3731 41 95 410, Fax: +49 3731 41 95 414

The contactless electrical characterization techniques MDP and MD-PICTS will be presented in this paper. Both methods are predestined for defect investigation in a variety of semiconductors. Due to a so far not reached sensitivity, major advantages of MDP are its high spatial resolution and its measurement speed, which allows for two dimensional inline measurements at production speed. Furthermore a versatile numerical tool for simulations of electrical properties of a semiconductor as a function of defect parameters was developed. MD-PICTS is a contactless temperature dependent measurement which allows the determination of activation energies of trap levels in the material. To demonstrate the abilities of both methods, measurements conducted at different semiconductor materials, e.g. silicon, silicon carbide, gallium arsenide and indium phosphide, will be presented exemplarily.

Copyright line will be provided by the publisher

42
43
44
45
46
47
48
49
50
51
52
53
54
55
56
57

1 Introduction and motivation In photovoltaic as well as in microelectronic industry the goal is to drive costs down by bringing yields up at the same time. To reach this goal it is important to analyze the defects existing in the used semiconductor materials and their impact on the latter device performance. Therefore the two contactless electrical characterization methods MDP and MD-PICTS for defect investigation are presented and results at different semiconductor materials are reviewed.

Due to the advanced microwave detection technique both methods have an advantage of sensitivity. As a consequence a high measurement speed is enabled. Mapping of 156 mm mc-Si wafer takes under a second [1]. The wide measurable injection range from 10^{10} to 10^{17} cm^{-3} is another benefit. Extraction of several defect parameters like the activation energy of the main recombination center from injection dependent investigations is possible. The high sensitivity is also used for measurements on lower qualitative materials or thin epitaxial layers on various substrates [2]. Using the varying penetration depth of light from different wavelength reveals even information about interface defects.

As one example the influence of metal contaminations as iron and chromium in silicon, diffusing into the material during the melting process and reducing the efficiency of solar cells and causing breakdowns of devices, is widely discussed in literature [3], as well as lifetime degradation caused by BO_2 [4]. MDP is a suitable tool for high resolution mappings of the density of iron as well as chromium and boron-oxygen-complexes. Furthermore due to high sensitivity and steady state measurements iron mapping in multicrystalline silicon bricks is even possible as inline

Copyright line will be provided by the publisher

measurement, revealing the concentration of all electrically active Fe.

MD-PICTS is an advancement of conventional photo induced current transient spectroscopy (PICTS) without the necessity of contacting the samples and with a higher sensitivity, opening new fields of applications on a variety of semiconductors revealing so far not accessible defect information. The technique is sensitive to defects acting as carrier traps while the DLTS method gives more information about the dominating recombination center in the material.

To achieve a better understanding of measured results a versatile numerical simulation tool was developed. It strictly starts from first principles rather than relying e.g. on SRH formalism and similar approximations. Application of this tool makes it possible to determine the impact of certain defect properties on important material parameters as minority carrier lifetime, photoconductivity or diffusion length. Thus it is used to simulate MD-PICTS and MDP measurements by taking different defects into account.

2 Experimental details

2.1 Microwave detected photoconductivity The novel method MDP is well suited for both, defect investigation by e.g. injection dependent minority carrier lifetime measurements, as well as mapping of wafers or even bricks for inline metrology. Its major advantage is the combination of sensitivity, resolution and speed, giving MDP the flexibility for a wide variety of different applications.

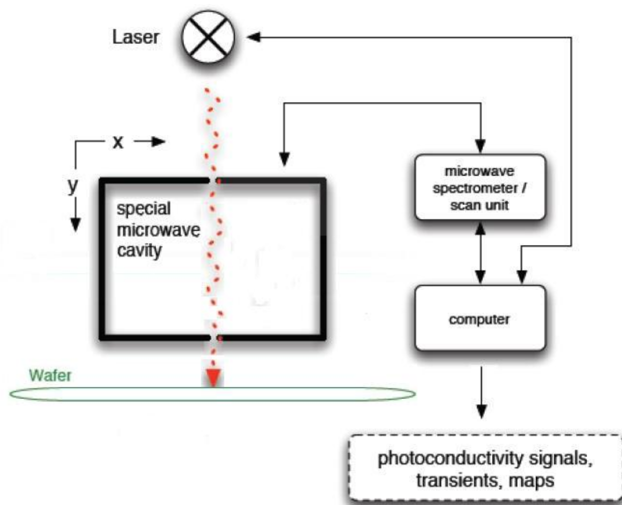

Figure 1 Scheme of MDP measurement setup.

The photoconductivity, which is closely related to the diffusion length, is measured by microwave absorption in a resonant microwave cavity, during and after the excitation with a rectangular laser pulse. Fig. 1 shows the layout of the MDP and MD-PICTS measurement setup. The sample is situated just outside the microwave cavity and is part of the measurement system. Thus, the complex dielectric constant of the sample influences the resonant frequency and the loss properties of the cavity. The microwave absorption by excess charge carriers is detected. The sample is placed on an x-y-table, allowing theoretically every sample size and to move the sample in the x-y-plane.

The high detection sensitivity enabled by this technique allows for injection dependent measurement over more than eight orders of magnitude depending on material under investigation with unlimited duration facilitating experiments in a non-equilibrium or steady state regime. Another major advantage of MDP is the ability to measure photoconductivity and minority carrier lifetime simultaneously. The minority carrier lifetime τ can be extracted from the semi logarithmic decay and the photoconductivity equals the signal height at steady state. Accordingly a variety of information can be gained from each measurement, like diffusion length, mobility and even trapping dynamics.

2.2 Microwave detected photo induced current transient spectroscopy For defect investigation on semiconductors deep level transient spectroscopy (DLTS) [5] and the photo induced current transient spectroscopy (PICTS) [6] are established techniques for more than twenty years. Both differ in their excitation mechanism and detection. While DLTS uses capacitive determination of excite charge reversal of defects caused by voltage pulses, PICTS measures the photoconductivity due to local irradiation with laser light. Therefore contacting of samples is required for both methods. Microwave detected photo induced current transient spectroscopy is an advancement of the conventional method, working contactless and therefore non-destructive.

To measure temperature dependent MD-PICTS, the MDP equipment shown in Fig. 1 is applied, with an additional cryostat for the sample. The setup allows for spatially resolved measurements.

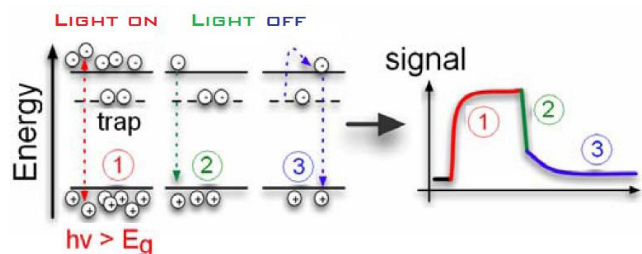

Figure 2 Physical processes and their corresponding signal parts in MD-PICTS: 1) generation and trapping of carriers, 2) fast recombination process, 3) thermal reemission of trapped carriers [8].

The method [7, 8] is based on the non-destructive investigation of photoconductivity signals by microwave absorption. Through pulsed light excitation provided by a la-

Copyright line will be provided by the publisher

ser excess carriers are generated in the material. According to intended investigation, wavelengths from UV- until the IR-range are applied, allowing for depth profiling as well as defect specific excitation with sub-band-gap wavelength. The light excitation causes a local rise of conductivity to a level dependent on the generation and recombination processes as well as on trapping and reemission dynamics (time interval 1 in Fig. 2). After the laser pulse is turned off the signal decreases rapidly caused by the fast recombination of the generated excess carriers (time interval 2). The slope of the so called transient depends on the recombination rate. This initial fast decay is followed by a slower decreasing part due to the reemission of trapped carriers into the associated band (time interval 3). Appropriate analysis leads to the extraction of defect parameters, e. g. the activation energy. After the photoexcitation, recombination and trapping of charge carriers the typical photoconductivity transient based on the thermal excited emission follows:

$$\Delta\sigma_{Transient} = q\mu\Delta n = q\mu n_{T_0}\tau_n \cdot e^{-e_{n_T}^t t} \quad (1)$$

n_{T_0} corresponds to the initial density of carriers trapped by a distinct defect, $e_{n_T}^t$ symbolizes the thermal excited emission rate of this trap and t is the time after the termination of the photo pulse. From $e_{n_T}^t$ the activation energy of a trap can be calculated using the relation

$$e_{n_T}^t = AT^2 \cdot e^{-\frac{E_A}{kT}}, \quad (2)$$

where A is a material constant.

For analysis the so-called two-gate technique according to DLTS is used leading to a similar defect spectra. MD-PICTS can be applied from semi-insulating samples to conductive ones. This opens characterization possibilities even on silicon which has not been possible with conventional PICTS. With the used cooling system the temperature range for MD- PICTS measurements is 80 to 500 K. Cooling down to 4 K is possible, but investigations suggest that liquid nitrogen temperature is sufficient for most defects. The filling pulse differs depending on the sample's properties between 10 and 1000 µs.

2.3 Materials and samples To show the potential of the contactless electrical characterization methods MDP and MD-PICTS, results from analysis of several semiconductor materials will be reviewed.

Shown MDP measurements for defect investigation are on passivated mc- and Cz-Si samples. For defect investigation by MDP-PICTS following samples were available: high quality 6 inch electronic grade p-doped monocrystalline silicon with a specific resistivity around 12 Ωcm; solar grade multi-crystalline p-type silicon from different parts of a brick; single-crystalline GaAs wafer from different preparations (vertical gradient freeze (VGF) and liquid encapsulated Czochralski (LEC)); InP samples from Fe-doped crystals with a resistivity between 0.01 and 2 x 10^8 Ωcm and semi-insulating 6H-SiC wafer grown by HTCVD with resistivities exceeding 2 x 10^9 Ωcm.

3 Simulations

During the development and application of MDP and MD-PICTS it became clear, that the obtained results are often not describable by simple defect models. The widely used SRH-Theory is only applicable if no trap influence is assumed, which is invalid especially for low injection measurements at e.g. mc-Si and MD-PICTS measurements in general, where this trap influence is investigated. This leads to the necessity of a new simulation tool without any approximations that is able to simulate injection and temperature dependent lifetimes as well as the trapping dynamics.

The numerical tool is based on a generalized rate equation system. The rate equations are used to describe the time dependent change of the carrier occupation of the bands ($\dot{n}, \dot{p}$) and defects ($\dot{n}_{Tj}$). All possible transitions between the defect levels in the forbidden gap and the bands of a semiconductor are described by transition rates.

A rate equation system is used, in which the only approximation is, that no direct interactions between defect levels are included [9].

$$\dot{n} = G_{BB}^o + G_{BB}^{th} + \sum_j \left(C_j - D_j\right) - U_{BB} - U_{Aug} \quad (3)$$

$$\dot{p} = G_{BB}^o + G_{BB}^{th} + \sum_j \left(F_j - E_j\right) - U_{BB} - U_{Aug} \quad (4)$$

$$\dot{n}_{Tj} = D_j + E_j - C_j - F_j \quad (5)$$

Based on the simulated time dependent carrier concentrations, the photoconductivity can be calculated using the mobility model of Dorkel and Leturcq [10]. The minority carrier lifetime finally can be extracted from the simulated transient decay of the photoconductivity after G_{opt} is set to zero or can be determined from the photoconductivity value, if a quasi steady state approach is used. Consequently the technique which is used to evaluate the lifetime values from the simulated data is strictly based on the used measurement technique and thus is correlated to the lifetime evaluation technique which is experimentally applied. Therefore a very good agreement between simulated values and measurement results is guaranteed. More details and a demonstration of the abilities of this simulation tool can be found in [11].

4 Experimental results and discussion

4.1 Microwave detected photoconductivity

Some of the most detrimental defects in silicon are traps in general, iron, boron-oxygen-complexes and chromium. All these defects have been investigated extensively in the last decades. With MDP it is possible to investigate these de-

Copyright line will be provided by the publisher

fects with a high resolution and by injection dependent lifetime measurements over a wide range of injections. Examples at passivated crystalline silicon wafers are presented.

With the ability of MDP to measure the lifetime and photoconductivity simultaneously, it is possible to estimate the trap density in mc-Si by the slightly modified model of Hornbeck and Haynes [12]. This model includes only one trap level, so that the determined trap density is only an estimation. By fitting the photoconductivity as a function of the optical generation rate, the trap density and activation energy can be determined. The following formula is used for the fitting:

$$\Delta\sigma = e \cdot \left[\Delta n(\mu_n + \mu_p) + \mu_p \frac{\Delta n \cdot N_T}{\Delta n + N_C \cdot \exp\left(\frac{-E_a}{kT}\right)_T} \right] \quad (6)$$

Fig. 3 shows an exemplary photoconductivity measurement at a mc-Si wafer, the fit-curve and the corresponding measured apparent lifetime.

By MD-PICTS measurements it is possible to separate different trap levels, but no information about the trap density is provided. By applying both methods a comprehensive study about traps in a sample can be conducted.

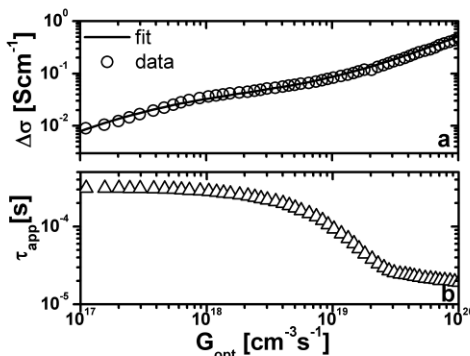

Figure 3: Measured photoconductivity and fit curve versus G_{opt} (a); apparent lifetime versus G_{opt} (b); determined trap parameter: $N_T = 8 \times 10^{14}$ cm^{-3}, $E_A = 0.387$ eV [13].

The iron detection by lifetime measurements is widely spread in the photovoltaic industry. The FeB pairs are dissociated by irradiating the sample with light and from the deviation between the measured lifetime before and after the dissociation the iron concentration can be determined via the following formula:

$$[Fe] = C_{Fe}\left(\frac{1}{\tau_{after}} - \frac{1}{\tau_{before}}\right) \quad (7)$$

The accuracy of this determination depends strongly on the use of an accurate calibration factor C_{Fe}, which depends on the injection, doping and trap density. By using the rate equation simulations it is possible to simulate the correct calibration factor for every possible measurement condition [13]. Fig. 4 shows an exemplary iron map of a mc-Si wafer with a resolution of 0.5 mm.

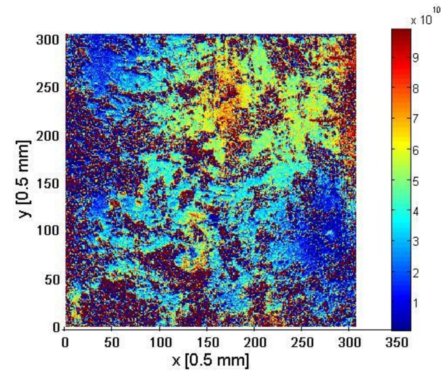

Figure 4 Exemplary iron map of a SiN_x passivated mc-Si wafer with a resolution of 0.5 mm.

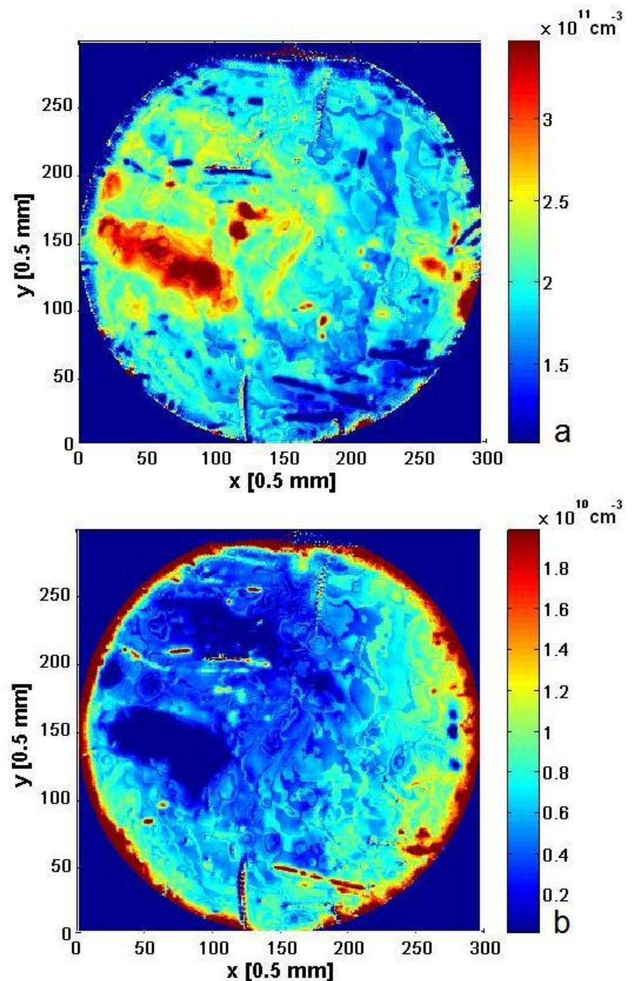

Figure 5 Relative BO_2 concentration (a) and Fe concentration (b) of an oxide passivated Cz-Si wafer.

Copyright line will be provided by the publisher

One difficulty of the iron detection is the separation from other defects, which also react on the irradiation with light, e.g. BO_2. With several annealing steps and repeated irradiation, it is possible to separate FeB and BO_2, since both defects differ in their association time constants and response to elevated temperatures. For the BO_2 determination also Eq. (7) is used, only with the calibration factor for BO_2 (C_{BO2}), which is simulated with the according defect parameters [14]. Since especially the carrier cross sections are not known exactly for BO_2, only a relative concentration can be measured. Fig. 5 displays the maps of the relative BO_2 and Fe concentration of an oxide passivated Cz-Si wafer. With these measurements typical differences in the distribution of both defects become obvious. Iron is concentrated at the edge of the sample, whereas BO_2 is distributed in high concentrated regions in the middle of the wafer. As mentioned above chromium is also an effective recombination centre in silicon. Similar to iron it occurs as CrB in boron doped silicon and can be dissociated to Cr_i and B by annealing the sample for 30 min at 250 °C. For the chromium determination also Eq. (7) is applied with a calibration factor C_{Cr}. An exemplary map of the relative chromium concentration of an intentionally chromium doped Cz-wafer is shown in Fig. 6.

By spatially resolved MD-PICTS measurements, it is possible to investigate the defect distribution of different regions of the here presented samples, in order to learn more about the correlation of e.g. BO_2 and thermal donors. An example of an investigation of thermal donors in silicon by MD-PICTS is presented in the next section.

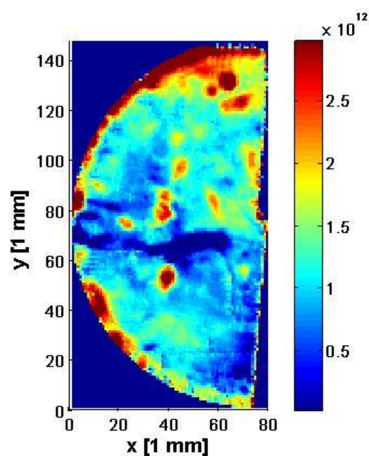

Figure 6 Exemplary map of the relative chromium concentration of an intentionally doped Cz-wafer.

4.2 Microwave detected photo induced current transient spectroscopy In contrast to DLTS a direct detection of metal contaminations like iron and chromium in silicon with PICTS is so far not successful because these defects are mostly acting as the main recombination centers. But by improving the sensitivity of a microwave detection system by several orders of magnitude the visualization of so far non-detectable defects in electronic grade silicon was achieved. One example is the electrical investigation of the well-known thermal donor (TD) in electronic grade p-doped silicon [15]. It is not detectable with deep level transient spectroscopy because of the position of the Fermi level. The MD-PICTS spectra in Fig. 7 shows two defect levels called PTD and PD. Following their evolution during thermal treatment suggests that the PTD peak refers to the thermal donors in silicon. After annealing for 40 minutes at 650 °C the emission maximum shifts more than 40 K to lower temperatures and is now located at 96 K (previously 133 K in the as-grown state and 140 K in the 450 °C treated sample). This is due to the change in capture cross section from $\sigma = 2 \times 10^{-18}\ cm^{-2}$ in the as-grown material to $\sigma = 2 \times 10^{-15}\ cm^{-2}$ in the 650 °C treated sample. The activation energy shifts only slightly from $E_A = 0.13$ eV to $E_A = 0.11$ eV. The change of position is believed to be caused by the transformation of an electrically active TD state into an electrically inactive trap state at temperatures above 600 °C [16]. At higher temperatures above 900 °C the intensity of the defect peak drops rapidly suggesting the dissociation of this defect level. A second defect level with $E_A = 0.26$ eV in as-grown samples at 242 K can be observed. It is caused by defects in the vicinity of dislocations. Correlations with PL measurements carry this assumption.

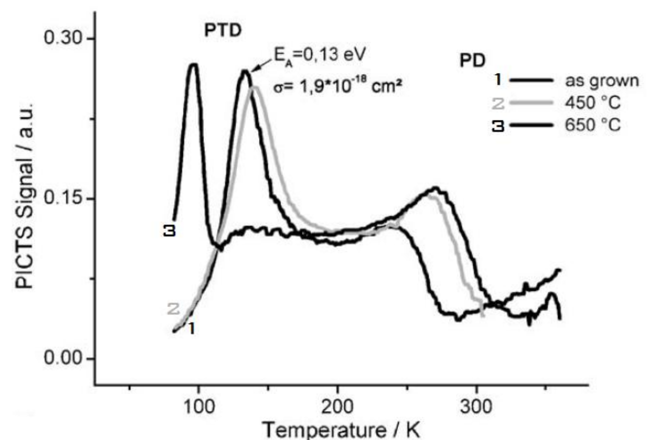

Figure 7 Spectra of temperature treated electronic grade p-doped silicon [15].

With MDP and MD-PICTS it is possible to obtain a deeper understanding of the observed sharp transition in the electrical properties of wafers prepared from different parts of a silicon brick [17]. The PTD and PD peaks known from electronic grade p-doped silicon and additional peaks are found by investigations of solar grade silicon samples (Fig. 8). P4 with an activation energy of 0.09 eV is only observable in the bottom part. Because of this low activation energy, the large width of the peak and the position of the corresponding wafer in the silicon brick it may be ascribed to a defect cluster containing nitrogen. P3, whose

Copyright line will be provided by the publisher

activation energy cannot be deduced, may have its origin in a cluster of bulk defects, because different surface treatments do not influence the peak. The appearance of all defect peaks differs from the associated brick position. Mapping the samples with MDP shows corresponding changes in lifetime, diffusion length and photoconductivity.

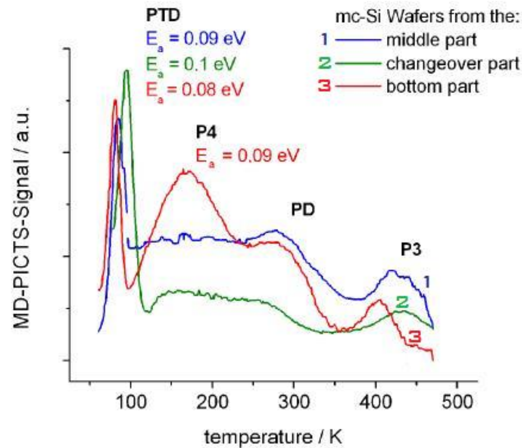

Figure 8 MD-PICTS spectra of solar grade p-doped silicon samples from different brick heights [17].

Beside investigations on silicon the new method for contactless electrical defect characterization was applied on gallium arsenide. MD-PICTS spectra show that a high density of the so-called EL5-defect in cell interior regions is responsible for dark areas of smaller lifetimes in MDP mappings [7]. In contrast to other techniques MD-PICTS can detect signals even from thin surface regions (0.3 µm) of SI GaAs samples and is therefore able to analyze e. g. influences of surface treatments. Fig. 9 shows the defect peak of the well-known EL2 defect in samples with different acceptor concentrations [18]. The activation energy varies between 0.55 eV and 0.73 eV which is in agreement with data from other groups [19, 20]. Conspicuous is the occurrence of the defect peak in positive and negative form.

The explanation of the negative PICTS peak effect is based on the system of rate equations from section 3, which calculates the carrier concentration of the involved energy levels by taking all participating generation and recombination processes as well as trapping and emission events during and after the photo excitation into account. Therefore photoconductivity signals, as they are measured as a result of the photo generation of carriers, can be simulated for different temperatures, if an appropriate mobility is taken into account. The consideration of the relevant donor and acceptor concentrations along with the concentration of the EL2 defect finally allows for the theoretical reproduction of experimental results. The latter show a dependence of the height of the EL2-related PICTS peak on the acceptor concentration in the material thus being associated with the Fermi level position. To briefly summarize the theoretical investigations it can be said that the fast recombination and trapping dynamics in the III-V-compound semiconductor GaAs lead to a drop of the electron concentration below the equilibrium value after the excitation is switched off, while the hole concentration shows a positive decay behavior. The amount of electrons that can be trapped and thus the ratio of the concentrations of the two types of excess carriers remaining in the bands ($\Delta n/\Delta p$) are determined by the initial occupation of the electron trap (EL2) and therefore by the position of the Fermi level. The resulting photoconductivity signal

$$\Delta\sigma = e \cdot (\mu n \Delta n + \mu p \Delta p) \tag{8}$$

is consequently controlled by the behavior of the dominant current fraction, thus also considering the large difference of the carrier mobility values for GaAs ($\mu n/\mu p \approx 20$). That means a positive decay behavior of the photoconductivity signal is only observable, if the excess hole concentration remarkably exceeds the excess electron concentration leading to signal

$$\mu n \Delta n < \mu p \Delta p. \tag{9}$$

This is the case for a Fermi level leaving most of the EL2 defect levels unoccupied [9].

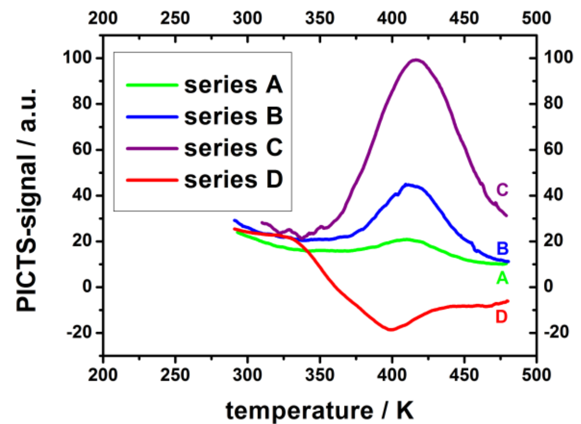

Figure 9 Detection of the EL2defect in SI GaAs samples with different acceptor concentrations by HT-MD-PICTS. Peak height and sign correlate to the acceptor concentrations [18]. Samples from series D were undoped, acceptor concentration rising from A to C.

Investigations on indium phosphide show that the defect content changes during annealing processes, which may also have an impact on the distribution of electrical properties. Whereas the defect content of as-grown samples depends on their position in the crystal, an equivalent set of defect levels is prominent in wafer-annealed samples [21]. Fig. 10 shows a comparison of Fe-doped SI-InP samples from different crystal positions. They differ in their characteristic defect levels. Additional negative peaks occur in some samples for temperatures above 350 K with the amplitude increasing with the crystal length. The oc-

Copyright line will be provided by the publisher

currence of peaks with different magnitude and sign in this temperature range is Fe-related. The negative peak is assigned to a transition of a hole leaving the Fe^{3+} level towards the valence band [22]. The observation of MD-PICTS signals of both signs in Fe-doped InP provided the first direct proof of iron acting as a recombination center in InP.

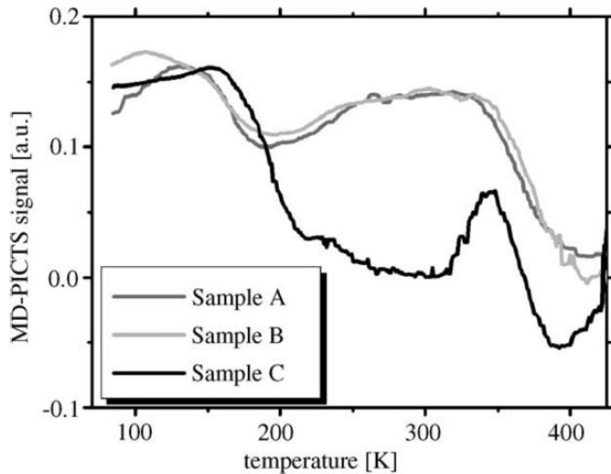

Figure 10 Comparison of MD-PICTS spectra of as-grown Fe-doped SI-InP samples from different crystal positions and thus different Fe-concentrations. The samples differ in their characteristic defect levels [21].

Analyses of semi-insulating 6H-SiC grown with a standard process and same process parameters show several differing shallow defect levels occurring in the low temperature range (Fig. 11). Additionally in samples grown under different C/Si-ratios different trap emission dynamics are obtained for higher temperatures, which are supposed to be due to different compensation effects [8]. The activation energies and capture cross sections of the defect peaks calculated from the spectra from Fig. 11 lie in the same range known from the literature [23-25]. They are traced back to omnipresent donor- and acceptor-like impurities and intrinsic defects.

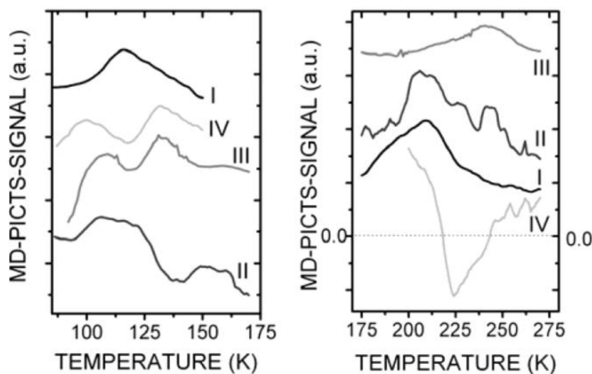

Figure 11 Comparison of MD-PICTS spectra of different SI-6H-SiC samples in different temperature ranges. Samples I-III were grown under same process conditions [8].

5 Conclusion The presented experimental results show the potential of the new methods MDP and MD-PICTS for contactless electrical characterization of defects in several semiconducting materials. Both techniques use the sensitivity benefit of microwave detection leading to a high spatial resolution and measurement speed as well as the possibility to recognize defects which were not investigated yet. A cooperation of MDP and MC-PICTS, e.g. mapping of a sample and analysis of several areas differing in reported lifetime with MD-PICTS for defect recognition, leads to insights of the cause of different measurable effects. The introduced simulation tool helps to get a deeper understanding of the experimental data. To demonstrate the abilities of both methods, a range of previous results on defect characterization were reviewed in this paper.

By determination of a calibration factor depending on injection level, doping and trap density MDP is a useful technique to map the local iron concentration with a high spatial resolution. Investigations on Cz-Si wafers show the typical differences in distribution of Fe_i and BO_2. While iron is concentrated at the edge of the sample, BO_2 is more distributed in the middle of the wafer.

With MD-PICTS experiments the visualization of so far non-detectable defects was achieved. One example is the investigation of the thermal donor defect level in electronic grade p-doped silicon. This defect cannot be obtained with DLTS because of the position of the Fermi level. Samples from solar grade mc-Si show different defect levels due to their brick height. Comparison between MD-PICTS spectra and lifetime mappings with MDP on gallium arsenide wafers lead to the assumption that lifetime degradation of several areas is caused by the EL5 defect. The EL2 defect was also analyzed. The differentiation between the single ionized state $EL2^+$ from the $EL2^0$ is possible with the help of the signal sign. Investigations on Fe-doped indium phosphide gave the first direct proof that iron acts as recombination centre in this material. In SI 6H-SiC the defect levels known from the literature were detected with similar activation energies and capture cross sections. A deeper understanding about the appearance of PICTS-signals of different signs with simulations basing on a rate equation system has been accomplished.

Acknowledgements The support of our research partner with the supply of samples and helpful discussions and also financial benefit is gratefully acknowledged. This work was also financially supported by the European Funds for Regional Development (EFRE) 2007-2013, the European Social Funds (ESF) 2007-2013 with the project number 080940489 and the State Saxony.

References

[1] K. Dornich, N. Schüler, D. Mittelstraß, A. Krause, B. Gründig-Wendrock, K. Niemietz, and J. R. Niklas, Proceedings of the 24th European Photovoltaic Solar Energy Conference, Hamburg, Germany, 2009, pp. 1106-1108.

Copyright line will be provided by the publisher

[2] K. Dornich, T. Hahn, and J. R. Niklas, Mat. Res. Symp. Proc. **864**, 549 (2005)
[3] A. A. Istratov, H. Hieslmair, and E. R. Weber, Appl. Phys. A **69**, 13 (1999).
[4] H. Fischer, and W. Pschunder, Proceedings of the 10th IEEE Photovoltaic Specialists Conference, Porto Alto, USA, 1973 pp. 404-411.
[5] D. V. Lang, J. Appl. Phys. **45**, 3023 (1974).
[6] O. Yoshie and M. Kamihara, Jpn. J. Appl. Phys. **22**, 621 (1983).
[7] B. Gündig-Wendrock, M. Jurisch, and J. R. Niklas, Mater. Sci. Eng. B **91-92**, 371 (2002).
[8] S. Hahn, F. C. Beyer, A. Gällström, P. Carlsson. A. Henry, B. Magnusson, J. R. Niklas, and E. Janzén, Mat. Sci. Forum **600-603**, 405 (2009).
[9] S. Schmerler, T. Hahn, S. Hahn, J. R. Niklas, and B. Gründig-Wendrock, J. Mat. Sci.: Mat. in Elect. **19**, 328 (2008).
[10] J. M. Dorkel, and J. P. Leturcq, Sol. Sta. Elect. **24**, 821 (1981)
[11] N. Schüler, T. Hahn, S. Schmerler, S. Hahn, K. Dornich, and J. R. Niklas, J. Appl. Phys. **107**, 064901 (2010).
[12] J. A. Hornbeck, and J. R. Haynes, Phys. Rev. **97**, 311 (1955).
[13] N. Schüler, T. Hahn, K. Dornich, and J. R. Niklas, Sol. Sta. Phen. **156-158**, 241 (2010)
[14] K. Bothe, R. Sinton, and J. Schmidt, Progr. in Phot. **13**, 287 (2005).
[15] K. Dornich, K. Niemietz, M. Wagner, and J. R. Niklas, Mat. Sci. Semicon. Proc. **9**, 241 (2006).
[16] A. Borghesi, B. Pivac, A. Sassalla, A. Stella, Appl. Phys. Rev **9**, 4169 (1995).
[17] K. Niemietz, K. Dornich, M. Ghosh, A. Müller, J. R. Niklas, Proceedings of the 21st European Photovoltaic Solar Energy Conference, Dresden, Germany, 2006, pp. 361-364.
[18] B. Gründig-Wendrock, K. Dornich, T. Hahn, U. Kretzner, and J. R. Niklas, Eur. J. Appl. Phys. **27 No. 1-3**, 363 (2004).
[19] K. Mojeiko-Kotlinska, H. Scibior, I. Brylowska, and M. Subotowicz, Phys. Stat. Sol (a) **138**, 217 (1993).
[20] S.-K. Min, E. K. Kim, and H. Y. Cho, J. Appl. Phys. **63**, 4422 (1988).
[21] S. Hahn, K. Dornich, T. Hahn, A. Köhler, and J. R. Niklas, Mat. Res. Soc. Symp. Proc. **9**, 355 (2005).
[22] S. Hahn, K. Dornich, T. Hahn, B. Gründig-Wendrock, B. Schwesig, G. Müller and J. R. Niklas, Proceedings of the MRS spring meeting, San Francisco, USA, 2005, pp. 573-578.
[23] A. A. Lebedev, Semiconductors **33**, 107 (1997).
[24] C. G. Hemmingsson, N. T. Son, and E. Janzén, Appl. Phys. Lett. **74**, 839 (1999).
[25] W. Suttrop, G. Pensel, and P. Lanig, Appl. Phys. A **51**, 231 (1990).

Copyright line will be provided by the publisher